Effects of soil properties and geomorphic parameters on the breach mechanisms of landslide dams and prediction of peak discharge

Citation for published version:
Guan, S, Shi, Z, Zheng, H, Shen, D, Hanley, KJ, Yang, J & Xia, C 2023, 'Effects of soil properties and geomorphic parameters on the breach mechanisms of landslide dams and prediction of peak discharge', *Acta geotechnica*. https://doi.org/10.1007/s11440-023-01908-2

Digital Object Identifier (DOI):
10.1007/s11440-023-01908-2

Published In:
Acta geotechnica

Effects of soil properties and geomorphic parameters on the breach mechanisms of landslide dams and prediction of peak discharge

Shenggong Guan[1], Zhenming Shi[1], Hongchao Zheng[1]*, Danyi Shen[1], Kevin J Hanley[2], Jiangtao Yang[1], Chengzhi Xia[1]

[1]Department of Geotechnical Engineering, College of Civil Engineering, Tongji University, China

[2]School of Engineering, Institute for Infrastructure and Environment, The University of Edinburgh, United Kingdom

*corresponding author: Hongchao Zheng, E–mail: 88zhenghongchao@tongji.edu.cn

Abstract

Breaching of a dam depends on the complex interaction between the dam and the backwater lake. Here, we conduct a series of experiments to investigate the failure mechanisms of landslide dams by considering debris composition and geomorphic parameters (dam height and lake volume), discern the failure mode and predict peak outflow rates of landslide dams in the field and in model tests. The failure modes of landslide dams are regulated by soil properties such as the shear strength and seepage. Failures of fine-grained and widely graded dams are induced by overtopping along with seepage instability and headcutting, respectively. Coarse-grained dams remain stable. Geomorphic parameters of dams govern the infilling time and affect the failure modes by the seepage. Seepage significantly reduces the stability of fine-grained dams and changes breach evolution and duration, while its effect on widely graded and coarse-grained dams is weak. Peak outflow rates of fine-grained dams are larger than those of widely graded dams with the same dam height due to larger breach depths and erosion rates. The peak outflow rate and breach duration are more related to the breach depth than the dam height because the influence of soil properties is considered in the former. Peak outflow rates of landslide dams are well predicted by a regression analysis with the lake volume, dam height and soil properties. Our results facilitate the understanding of breach mechanisms of landslide dams and prediction of peak outflow rates based on dam parameters.

Keywords: Landslide dams, failure mode, soil properties, geomorphic parameters, peak outflow rate

1. Introduction

Landslide dams develop when rivers are blocked by debris material from landslides, avalanches, and debris flows [31, 13, 39, 41, 42]. Landslide dams are often induced by strong earthquakes, cloudburst and snowmelt caused by climate warming, threatening life and property downstream [19, 27, 29]. For example, the Baige landslide dam breached on 12 November 2018 and the peak discharge was up to 33,900 m^3/s [40].

The failures of landslide dams depend on complex interactions between dam characteristics such as debris composition and dam geometry, and the hydrological parameters of the river like lake volume and inflow rate [13, 2]. The research shows that dams usually breach by overtopping and headcutting [7, 46, 8, 43]. Dam failures directly caused by seepage occur relatively infrequently. Landslide dams are usually composed of weakly sorted debris with a wide grading (micrometers to meters), constraining the development of seepage channels [27]. The longevity of a dam is often smaller than the time for seepage channels through the dam to develop due to a large dam width [29]. The failure mode is regulated by debris strength and its permeability [9, 26]. The influence of debris type on the failure mode for landslide dams has been investigated through a series of laboratory tests [16, 17]. The infilling stage from dam formation to breaching largely depends on the geomorphic parameters of a dam and backwater alters debris strength by the seepage. However, the effect of geomorphic parameters and dam composition on the failure mode is rarely explored.

Landslide dam stability is significantly affected by the backwater lake, dam geometry and the debris composition [12]. At present, the dam's stability is evaluated by the use of the geomorphic parameters of the river and dam [19]. The blockage index proposed by Canuti et al. [4] indicates the correlations of the basin area and landslide volume to the landslide dam stability. The dam height is incorporated in the blockage index proposed by Ermini and Casagli [12] and Korup [19] because overtopping and seepage gradient in a piping passage are closely related to the dam height. The hydromorphological stability index presented by Stefanelli et al. [33] is based on destabilization of the dam by the flowing river. Nevertheless, the potential correlations between debris composition and the stability of a dam are rarely considered.

Prediction of peak outflow rate is crucial to evaluate the risk posed by a breaching flood. Costa and Schuster [11] conducted the first widely known estimation by means of an empirical model considering the drop of water level or lake volume and dam height. Subsequently, lake volume, dam height and dam erodibility have been used to calculate the peak outflow rate by regression analysis for landslide dams in the field [22]. In addition, physically based models employ the theories of hydraulics and soil mechanics to obtain the development process of a breach and the corresponding discharge hydrograph. For instance, Chang and Zhang [5] propose a DABA model and Zhong et al. [44] present a DB-IWHR model which is applied to the breach simulation of landslide dams. The erosion rate of the dam debris and rate of breach development are commonly obtained using empirical equations in these physical models. Prediction of peak breach discharge based on available parameters is still challenging.

A series of tests were conducted to analyze the failure mechanisms of landslide dams with different debris compositions and geomorphic parameters and investigate the failure modes and outflow rates. The structure of this study is as follows. The experimental equipment, debris composition and experimental objective are first presented. Subsequently, we analyze the breach processes and failure modes of landslide dams. Correlations between the breach parameters and dam parameters obtained from tested dams and landslide dams in the field are presented. Finally, we compare the longitudinal evolutions of fine-grained and widely graded dams, the potential breach risk of the residual dams, and the effects of debris composition and dam height on the peak outflow rate.

2. Materials and Methods

2.1 Experimental equipment

The experimental flume includes an impounding reservoir, a water injection pump and a drainage pump (both with maximum flow rates of 0.1 m^3/s), and straight chutes. The drainage pump was used to discharge the water at the downstream of the dam. Two chutes were adopted in these tests: a bigger chute of 42 m length, 0.80 m width and 1.25 m height; a smaller chute of 5.0 m length, 0.40 m width and 0.4 m height. The sidewalls of both chutes were made of transparent tempered glass and thus breach processes of landslide dams can be recorded. The bottoms of both flumes were horizontal, considering the Tangjiashan landslide dam had a low longitudinal grade (0.006) during breaching [23]. An electromagnetic flowmeter was utilized to control the inflow rate of the upstream reservoir.

The breach process and the upstream water level of the dam were recorded by a camera (EOS550D, Canon, 3456 x 5184 pixel) and a video camera, respectively, at the side of each chute (Fig. 1). The breach discharge was calculated using photographs taken by the camera combined with a steel tape. The overflow process of a dam-break flood was recorded by two video cameras (GZ-R10BAC, JVC, 1080 x 1920 pixel) above and downstream of the dam in each flume.

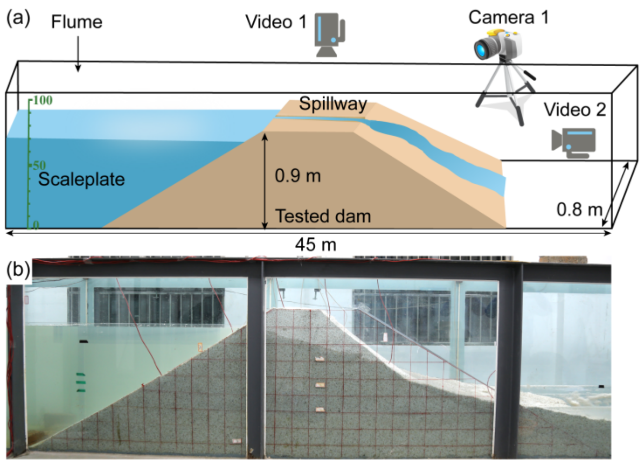

Fig. 1. Experimental apparatus: (a) schematic diagram of the model dam in the larger flume with a length of 42 m; (b) photograph of the fine-grained dam (test F1). The grid in red was used to delineate the section development of a dam.

2.2 Dam materials

As shown in Fig. 2, grain distributions of the model dams were derived from landslide dams in the field. Three debris compositions termed widely graded, fine-grained, and coarse-grained were obtained based on the Tangjiashan, Hsiaolin and Xiaogangjian landslide dams, respectively [5, 20]. The definition of debris types was based on the dam material which is inconsistent with the standard engineering classification of soils [32]. The median particle sizes d_{50} of the widely graded and fine-grained debris were significantly smaller than the values for the coarse-grained debris (Table 1).

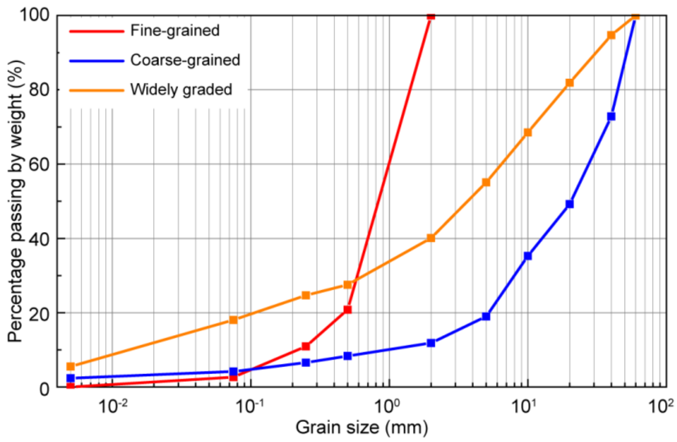

Fig. 2. Grading curves of debris material in tested dams.

Each tested dam had a dry density ρ_d of 1780 kg/m^3, matching the drillhole data of in-field dams [5]. gravel (2–60 mm), sand (0.075–2 mm) and Silt (0.005–0.075 mm) were mixed to prepare the dam debris, as shown in Fig. S1. The maximum particle size was 60 mm (coarse gravel) for coarse-grained debris whereas the value was 2 mm (coarse sand) for fine-grained debris as recommended in the current specification of soil test [32]. The mass of the model dam was calculated by the dry density and dam volume. Then, the masses of the different debris fractions were obtained.

Geotechnical properties of the dam debris were evaluated. The hydraulic conductivities k of the debris were obtained by constant-head permeability tests at the same dry density as the tested dams (Table 1). The values of k for widely graded and fine-grained debris were significantly smaller than that of coarse-grained debris. The shear strengths of debris materials were obtained by large-scale triaxial tests (GCTS, 600 mm x 300 mm). All debris was cohesionless. The internal friction angles φ of widely graded and fine-grained debris were smaller than that of coarse-grained debris.

Table 1. Geotechnical properties of dam debris

Dam material	ρ_d (g/cm^3)	d_{50} (mm)	C_u	C_c	c (Pa)	φ (°)	k (10^{-4} m/s)
Fine-grained	1.78	0.8	5.5	1.2	0	26.8	2.0
Widely graded	1.78	3.7	61.3	0.7	0	37.8	3.3
Coarse-grained	1.78	20.7	28.7	2.5	0	43.1	248.0

Note: C_c and C_u are the curvature coefficient and uniformity coefficient of the grading curve, respectively. φ and c are the internal friction angle and cohesion, respectively.

2.3 Experimental objective

The tests aimed to investigate the failure mechanisms of landslide dams, discern the failure modes of the dams with different debris, and analyze the effects of the dam and lake parameters on the breach process and peak outflow rate. The relevant parameters used in the tests were debris composition (widely graded, fine-grained and coarse-grained), dam height, and volume of the upstream lake (Table 2). A total of eleven tests were conducted.

Table 2 Characteristics of the different tests

Test	Debris material	h_d (m)	b_l (m)	V_u (m^3)	c_d	c_l
F1	F	0.90	26.5	19.1	1.3	3.0
F2	F	0.40	26.5	8.5	1.7	5.1
F3	F	0.24	2.0	0.2	1.6	2.4
F4	F	0.90	11.9	8.5	1.3	2.3
F5	F	0.90	11.9	8.5	1.3	2.3

W1	W	0.90	26.5	19.1	1.3	3.0
W2	W	0.40	26.5	8.5	1.7	5.1
W3	W	0.24	2.0	0.2	1.6	2.4
C1	C	0.90	26.5	19.1	1.3	3.0
C2	C	0.40	26.5	8.5	1.7	5.1
C3	C	0.24	2.0	0.2	1.6	2.4

Note: C, F, and W represent the coarse-grained, widely graded and fine-grained dams, respectively. h_d is the dam height. b_l and V_u are the length and volume of the backwater lake, respectively. c_d is the dam shape coefficient which is equal to the cubic root of the dam volume divided by height. c_l is the lake shape coefficient which is equal to the cubic root of lake volume divided by dam height. F4 and F5 are repeated tests with the same experimental parameters.

The debris grading in tests F1–F5, W1–W3 and C1–C3 were fine-grained, widely graded and coarse-grained debris, respectively. The dams with heights of 0.90 m and 0.40 m were tested in the larger flume. The lengths of the upstream reservoirs were determined to be 26.5 m and 11.9 m for varying lake volumes by comparing F1–F2 and F4–F5. The dams with heights of 0.24 m were tested in the smaller flume with a fixed length of the upstream reservoir of 2.0 m. The aim was to analyze the effect of infilling time before overflow on the failure mode by comparing dams in the larger and smaller flumes. The inflow rate was 1 L/s for all tests.

Natural dams commonly have geometrical parameters varying over a wide range [40]. Thus, a prototype dam was not selected in this study. The length of trapezoidal dams was equal to the flume width. For a natural landslide dam, the upstream and downstream slopes vary from 11°–45° [40]. Here, the slope angles of the dams were determined to be 30° for all tests. The crest widths were 0.50 m for dams with a height of 0.9 m. The crest widths of dams with heights of 0.40 m and 0.24 m were reduced in proportion to the dam height, compared to the dams with heights of 0.9 m. The dam shape coefficients c_d of 1.3–1.7 and lake shape coefficients c_l of 2.3–5.1 of tested dams matched the values for natural landslide dams [45]. This indicated that the dam geometries satisfied scaling laws. A rectangular groove with a width and depth of 0.05 m was excavated on the dam crest for the simulation of the artificial spillway that is usually used to reduce the peak outflow rate of a landslide dam (Fig. 1).

2.4 Experimental procedure

The test process is as follows:

(1) The outline of each dam was depicted on the flume sidewall by use of a grease pencil.

(2) Dams were prepared in layers. The thickness of each layer was 0.1 m for dams with heights of 0.9 m or 0.4 m; the equivalent value was 0.08 m for dams with heights of 0.24 m.

(3) The inflow rate was 1 L/s throughout the experiment. The outflow water from the dam was discharged by the dewatering pump. Snapshots from still and video cameras were automatically stored.

(4) The failure mode of a tested dam was obtained from the recorded pictures. The stage hydrograph was delineated from the snapshots and the outflow rate was obtained from the stage hydrograph based on the continuity equation [43]. The

geometry of the deposition after dam breaching was measured with a ruler.

3. Breach processes and failure modes of landslide dams

Firstly, the failure processes of landslide dams are introduced in this section. The influence of seepage on the failure modes and stability of landslide dams is then evaluated. Finally, the deposition characteristics of landslide dams after breaching are presented.

3.1 Breach processes of landslide dams

3.1.1 Breach processes of fine-grained dams

The fine-grained dam in test F1 had a height h_d of 0.9 m (Table 2). With the upstream water level h_u = 0.07 m, the water seeped through the downstream slope face of the dam. Affected by the seepage flow, the debris close to the downstream toe was eroded away when h_u = 0.14 m. As shown in Fig. 3, the dam slope in the downstream direction below the phreatic line was partly liquefied and increasingly entrained and its slope angle reduced to 15–20°. The reason was the shear strength of fine-grained debris (Table 1) was lower than the sum of the sliding stress generated by gravity and seepage stress. The dam slope above the phreatic line continually slid and collapsed, forming an almost-vertical free face (Fig. 3a). This reduced the width of the dam crest before outflow. Thereafter, the water flowed through the breach and a turbid hyperconcentrated flow was developed by entraining the fine-grained debris. An overtopping failure of the dam was thus initiated. This breach quickly widened in both the cross-stream and stream-flow directions, lowering the dam height. The breach retained its trapezoidal shape with an angle of 45–60° during overtopping. This slope angle was greater than the φ value of fine-grained debris because of the lateral pressure applied by the overflow. Finally, clear water flowed over the dam site, indicating the residual dam was not entrained by the overtopping flow.

The dam-breaching processes in tests F2–F5 were the same as in test F1 (Fig. S2). The heights of the almost-vertical free faces in tests F1 and F2 were larger than that in test F3. This is because the dams in tests F1 and F2 had larger lake volumes (Table 2) and sufficient time to form the free face before dam breaching. Regardless of the lake volume and dam height, the fine-grained dams in tests F1–F5 failed by overtopping along with seepage instability.

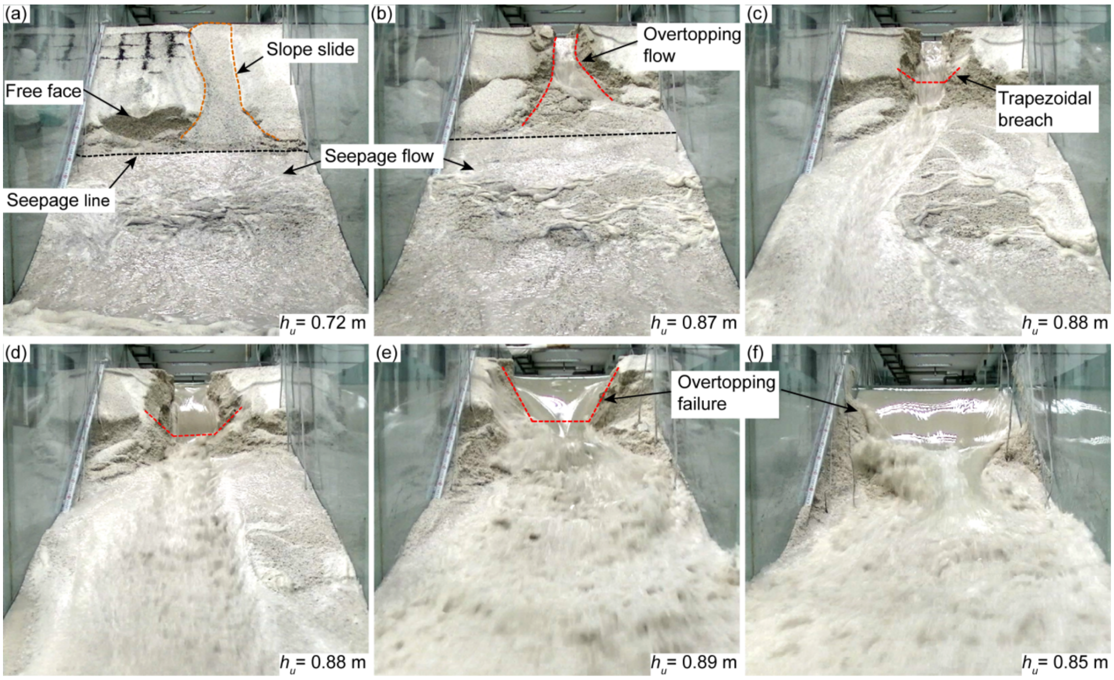

Fig. 3. Breach process of the fine-grained dam in test F1. The width and depth of the trapezoidal breach rapidly increased and the dam height decreased due to the outburst flood.

3.1.2 Breach processes of widely graded dams

As shown in Fig. 4, the fine debris around the dam toe was eroded away by seepage and the coarse debris was stable for the widely graded dam in test W1. As a result, a piping channel was not observed. The angle of the downstream dam slope was approximately its initial value (30°). This process was different from that of fine-grained dams because widely graded debris had a larger φ value (Table 1).

When water overflowed through the breach, headcutting occurred when the critical shear stress with respect to debris initiation was exceeded on some part of the downstream dam slope. Fine sand and silt were entrained by the flood, indicated by the milky outflow, while few coarse gravel grains were eroded. A channelized flow occurred which conversely enlarged the depth and width of the breach. The channelized outflow rate was increased by this positive feedback. The channel head progressively migrated toward the dam crest with a consequent entrainment of debris material. Some coarse debris was first initiated and then deposited around the dam toe, leading to the deflection of the channel. A waterfall and stepwise structure, termed a 'cascading step' by Wang et al. [34], was developed because coarse gravel was more difficult to carry away than finer debris due to a large uniformity coefficient of debris material (Table 1). The cascading-step structure is observed for the Yujunmen and Tiger-leaping Gorge landslide dams [34, 35]. During headcutting migration, the breach depth and dam height remained nearly unchanged. The side slope of the breach collapsed when the channel head arrived at the upstream dam's slope face and the dam height significantly decreased. The lateral slope had a smaller expansion rate than the vertical slope, leading to a growth of the breach angle. The breach was nearly vertical in the cross-stream direction and even toppling failure occurred.

The time from the overflow to the breach termination (550 s) in test F1 was significantly lower than the value (2540 s) in test W1 due to the migration of the headcutting. Here, dam breaching was terminated when the dam was not entrained by the outburst flood. The shape of the channel in the stream direction was analogous to an hourglass. This breach behavior was also observed for the Tangjiashan landslide dam [5]. The failure processes of the dams in tests W2–W3 in Fig. S3 were the same as in test W1. The dam toe was carried away in tests W1–W2 before overflowing. However, this phenomenon did not occur in test W3 considering that time for the seepage is relatively limited. Regardless of the dam height and lake volume, widely graded dams failed by headcutting.

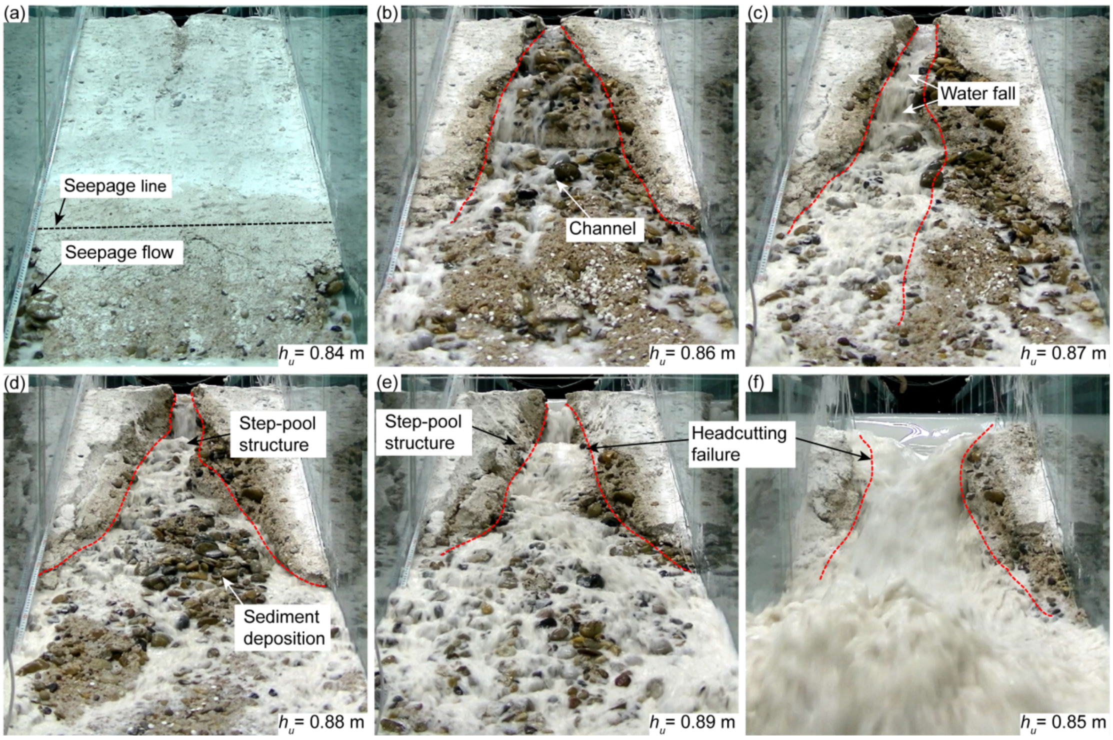

Fig. 4. Breach process of the widely graded dam in test W1. Headcutting occurred on the downstream slope face of the dam. The depth and width of the breach and the dam height remained nearly unchanged during headcutting migration.

3.1.3 Stable dams composed of coarse-grained debris

As shown in Fig. 5, the inflow rate amounted to the seepage rate for the coarse-grained dam in test C1 when the upstream water level rose to 0.34 m because of a high hydraulic conductivity (Table 1). Overflow was not observed in contrast to the processes of fine-grained and widely graded dams. Affected by a smaller dam height and seepage rate for tests C2 and C3, overtopping was developed (Fig. S4). The dams remained stable for more than 4 hours although fine debris on the downstream slope of the dams was carried away. This is because the maximum outflow rate was nearly 0.5 L/s and coarse debris could not be eroded by the shear stress applied by the overflow.

When the inflow rate increased to 2 L/s, dams in tests C2 and C3 failed by overtopping. By contrast, the upstream water depth increased to 0.48 m for the dam in test C1, after which the dam remained stable. This is consistent with the Xiaogangjian landslide dam composed of coarse-grained debris [10] that remained stable for nearly a month until a spillway was excavated by blasting. The Usoi landslide dam composed of coarse-grained debris triggered in 1911 in the Bartang River is still stable with a seepage rate of 46–47 m^3/s [25].

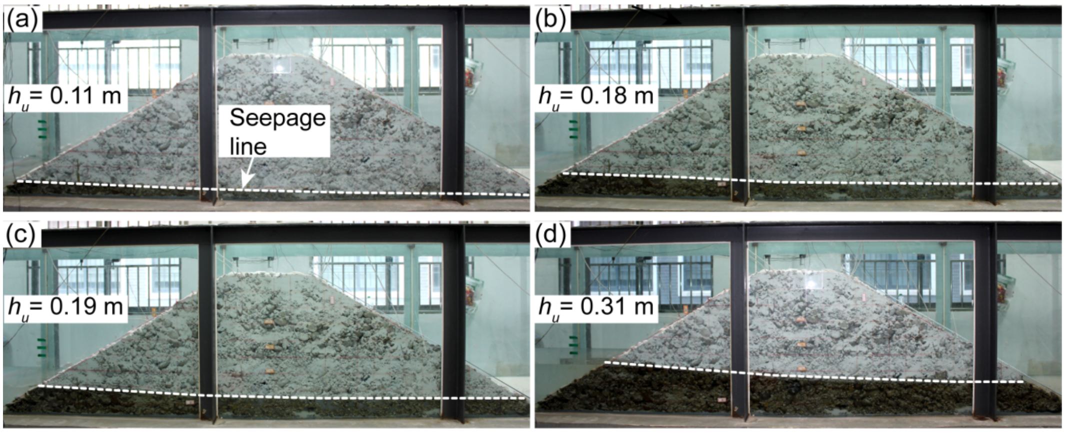

Fig. 5. Stable dam composed of coarse-grained debris in test C1. The inflow rate and seepage rate were balanced at an upstream water level of 0.34 m. White dotted lines denote the phreatic lines through the dam.

3.2 Effects of seepage on the stability of landslide dams

With increasing upstream water level, phreatic lines rose from the dam foundation to the dam crest (Fig. 6). The phreatic lines were nearly linear in the stream flow direction for fine-grained and coarse-grained dams. By contrast, they were stepwise for widely graded dams, possibly caused by the large uniformity coefficient of debris material. The phreatic lines through the dams gradually steepened due to the decrease of infiltration length and increase of water level. The average angles of the phreatic lines increased up to 20° for fine-grained and widely graded dams, while they were nearly horizontal for coarse-grained dams (0.05°) due to a high hydraulic conductivity.

The breach process of a landslide dam can be instigated by the seepage stress because the stability of a downstream dam slope is reduced. An equilibrium analysis was conducted to assess the stability coefficient s of a dam slope affected by seepage stress f_s (Fig. S5).

$$s = \frac{R_s}{F_s + f_s} \tag{1}$$

where F_s is the sliding stress expressed as

$$F_s = \rho_d g h \sin\alpha \tag{2}$$

where α is the slope angle and h is the slide thickness; g is the acceleration of gravity; R_s is the resistance stress

$$R_s = c + \sigma \tan\varphi \tag{3}$$

where σ is the effective stress in the normal direction. f_s is obtained by

$$f_s = \rho_w g h i \tag{4}$$

where ρ_w is the water density and i is the hydraulic gradient.

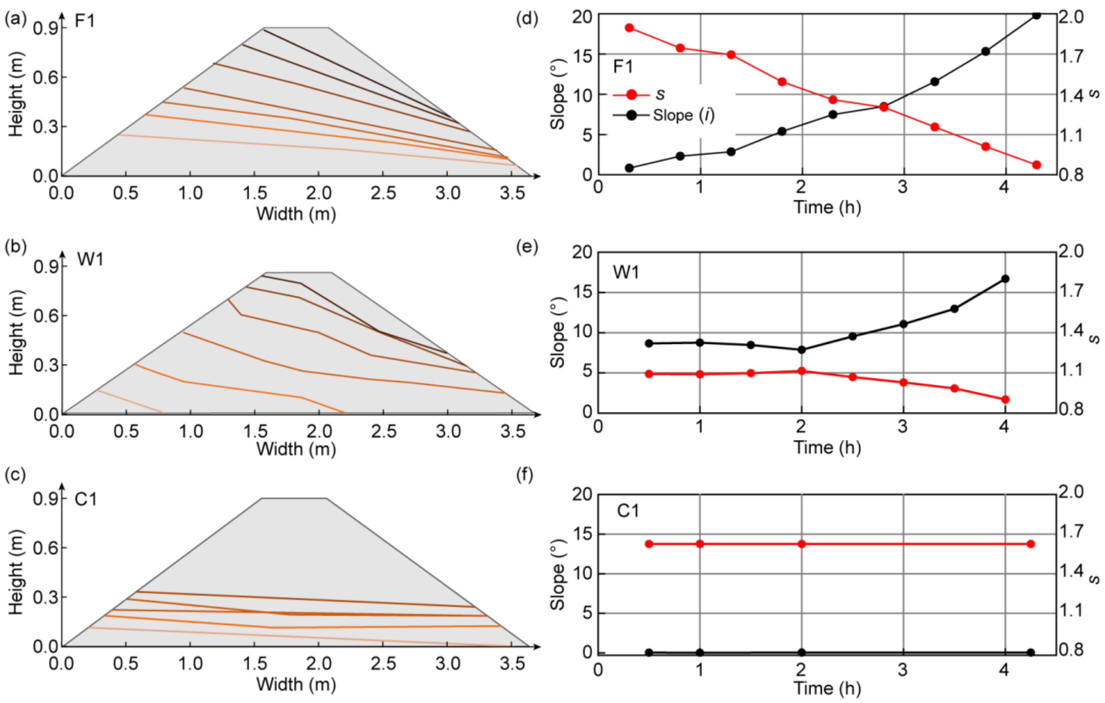

Fig. 6. Phreatic lines and stability coefficients s of downstream dam slopes in tests F1, W1 and C1. The hydraulic gradient i is the average slope of the phreatic line. The downstream slope angles of the dam α decreased to 15° for test F1 and α = 30° for tests W1 and C1 before overtopping.

The failure modes of landslide dams were regulated by the debris strength and seepage. The stability coefficient s of the dam in test F1 decreased from 1.9 to 0.9 with the increase of hydraulic gradient i (Fig. 6d). The downstream dam slope reached a critical state for instability before overtopping. Fine-grained debris was prone to be carried away by the outflow. The size of the breach rapidly broadened and dam height was reduced due to the low shear strength and slope stability (Fig. 7a). The overtopping failure along with seepage instability was thus induced. s slightly decreased for the dam composed of widely graded debris in test W1. Due to a high shear strength, finer debris was washed away to leave coarse gravel behind on the dam slope face, leading to the cascading-step structure (Fig. 7b). The stability coefficient is suitable for relatively uniform fine-grained dams rather than widely graded dams with partial failure. Dam height quickly decreased after the headcutting reached the upstream slope of the dam. As a result, widely graded dams failed by headcutting. Due to a high hydraulic conductivity, seepage stress had a negligible effect on the coarse-grained dam in test C1 and s remained at 1.6. The dams were stable although overflow occurred for tests C2 and C3.

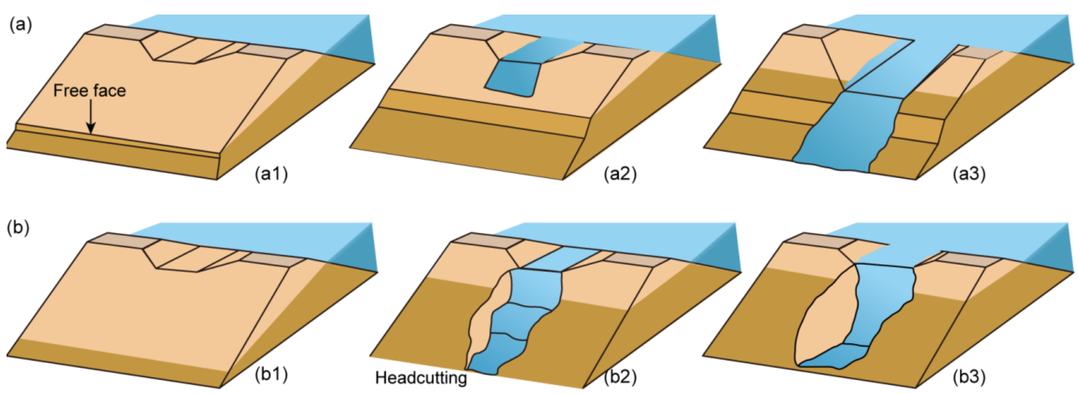

Fig. 7. Failure modes of landslide dams during breaching: (a) overtopping failure

along with seepage for fine-grained dams; (b) headcutting failure for widely graded dams.

3.3 Deposition of landslide dams after breaching

A residual dam usually existed after dam breaching due to a large dam volume [40]. The deposit thickness of the residual dam in test F1 slowly reduced at an angle of 2.6° in the direction of flow while it showed a stepwise decrease for the dam in test W1 (Fig. 8). The overall slope angle of the residual dam in test W1 (4.5°) was larger than for test F1. The debris grains deposited in test F1 were uniformly distributed due to a low uniformity coefficient (Table 1). However, an armoring layer composed of coarse gravel developed on the surface of the deposition in test W1 due to the grain segregation induced by the outburst flood. These observations were also applicable for the depositions in tests W2–W3 and C2–C3. This armoring layer first occurred near the dam toe and then gradually extended in the stream direction. This armoring layer, termed a 'boulder bar', was observed near the river bank after the Yigong landslide dam breached [36].

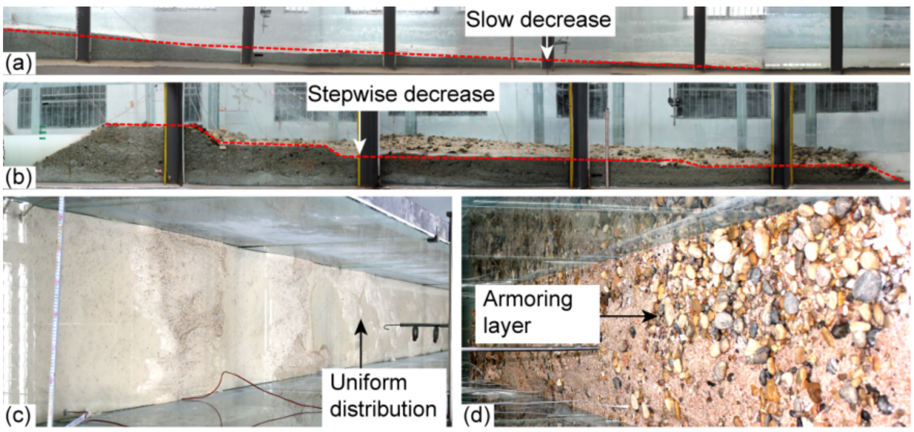

Fig. 8. Deposition of landslide dams after breaching. (a) and (c) Side and vertical

views of residual dams in test F1; (b) and (d) Side and vertical views of residual dams in test W1. The stream direction in the pictures is to the right.

The height of the residual dam h_r, defined as the maximum deposit thickness, was nearly one-third of the dam height h_d in test F1 (Figs. 9a and b). It was similar for the dams in tests F2 and F3. Widely graded dams had a larger h_r than fine-grained dams with the same h_d because of a high shear strength of widely graded debris. h_r were approximately half of the dam height for tests W1–W3. This is consistent with the Tangjiashan landslide dam composed of widely graded debris with h_d = 82 m and h_r = 37 m [5]. The length of residual dam l_d increased with the increase of h_d for fine-grained and widely graded debris due to the increase in dam volume. l_d of fine-grained dams were longer than those of widely graded dams (Figs. 9c and d). The geometric parameters of residual dams were regulated by critical erosive shear stress τ_c. Widely graded debris had a higher τ_c than fine-grained debris, as indicated by the empirical equations proposed by Neill [21] $\tau_c = 0.7609\gamma_w\left(G_s - 1\right)d_{50}{}^{2/3}h_w{}^{1/3}$ and Annandale [1] $\tau_c = \frac{2}{3}gd\left(\rho_s - \rho_w\right)\tan\varphi$, where γ_w is the unit weight of water, G_s is the specific gravity, h_w is water depth, and ρ_s is the grain density. The ratio of l_d to h_d increased first with dam height and then decreased for fine-grained and widely graded dams. The reason is that the lake shape coefficients c_l in tests F2 and W2 (Table 2) were larger than those in tests F1 and F3, W1 and W3 and the stream power used to transport debris grains by the outburst flood was higher.

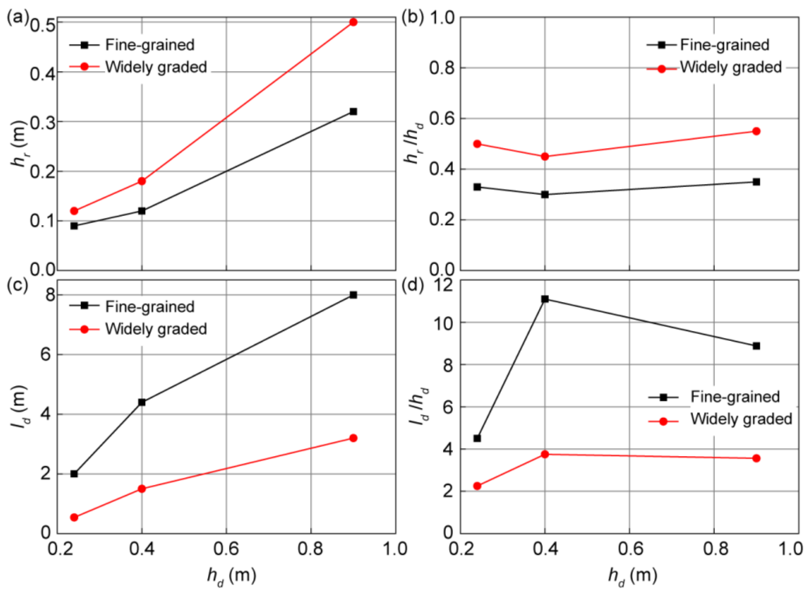

Fig. 9. Relationships between the length l_d and height h_r of the residual dam and the dam height h_d in tests F1–F3 and W1–W3. l_d is defined the distance between the toe of the downstream dam slope and the deposition end. h_r is defined as the maximum deposit thickness.

4. Breach parameters of landslide dams

4.1 Discharge hydrographs of landslide dams

The discharge hydrograph of a landslide dam changed with breach development (Fig. 10). When overtopping flow passed through the breach in the initial stage (Fig. S6), the flow velocity and depth were small (Figs. 3 and 4). The breach slowly broadened, leading to a low growth in outflow rate. The time for breach initiation of fine-grained dams varied in the range of 15–19 s for different dam heights. The reason is that dam slope failure caused by seepage was obvious for dams with h_d=0.4 m or 0.9 m. In contrast, the initial stage durations of widely graded dams significantly increased with the increase of the dam height by comparing tests W1–W3. Widely graded dams had a longer initiation time than fine-grained dams with the same dam height due to headcutting migration. In the development stage, the breach was rapidly enlarged in both lateral and vertical directions when the height at the upstream dam slope decreased. The outflow rate sharply increased and then decreased, displaying an approximately symmetrical hydrograph (Fig. 10).

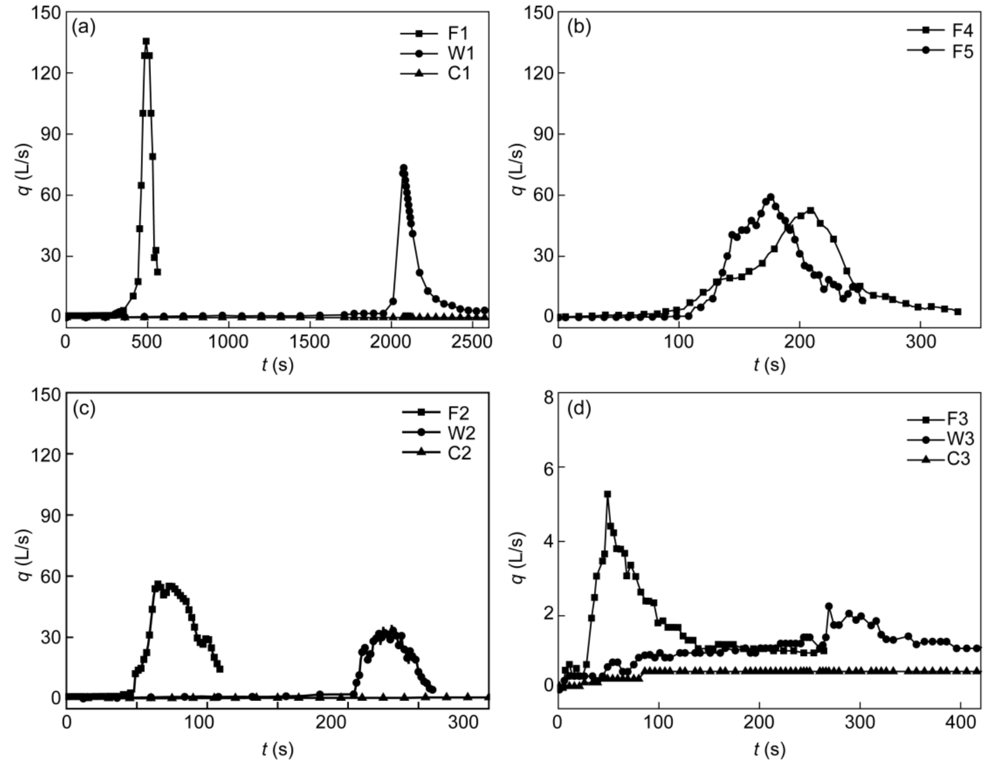

Fig. 10. Discharge hydrographs of landslide dams. The outflow rate in test C1 remained at zero. The outflow rates in tests C2 and C3 were smaller than the inflow rates because these dams remained stable.

The peak outflow rate q_b of the dam in test F1 (135.1 L/s) was the highest; by contrast, q_b was zero for test C1. The discharge hydrographs and breach process of the dams in tests F4 and F5 were highly consistent, indicating the repeatability of the test results. q_b of fine-grained dams were larger than those of widely graded dams with the same h_d. This is because the residual dam heights of fine-grained dams were smaller and much of the lake volume was released during breaching (Fig. 9). Furthermore, the mean erosion rates E of the fine-grained dams in the breach development stage were higher than those of widely graded dams (Fig. 11). The peak outflow rate for the fine-grained dam in test F2 was 56.7 L/s, matching the values for the dams in tests F4 and F5 (59.1 L/s and 52.5 L/s) due to the same lake volumes (Table 2). The outflow rates were smaller than the inflow rates in tests C1–C3 because coarse-grained dams remained stable.

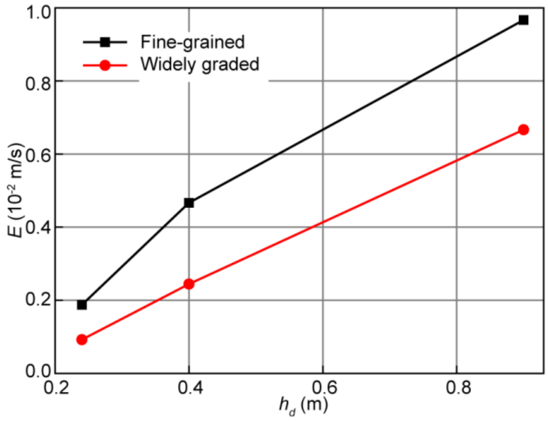

Fig. 11. Mean erosion rate E of fine-grained and widely graded dams in the development stage versus the dam height h_d.

Widely graded dams had multiple peaks in the discharge hydrographs (Fig. 10). This is because a cascading-step structure developed for a widely graded dam. The small debris on the breach bottom was carried away and the coarse gravel was left over. Thus, the outflow rate increased first and then decreased, leading to a peak in the discharge hydrograph. After the coarse gravel was scattered and washed away, the breach was undercut by the overflow and then another peak outflow rate appeared. Multiple peaks can also occur in the discharge hydrographs of fine-grained dams. The reason is the breach was intermittently blocked by the collapse of the side slope. Compared with widely graded dams, fine-grained dams had a lower φ value and thus a higher trend to slide into the breach, leading to multiple peaks.

4.2 Relationship between dam parameters and breach parameters

The breach of a landslide dam is regulated by the interaction between the dam and the backwater lake [13]. The correlations between the breach parameters and dam parameters were explored by comparing parameter values of dams in the field and in model tests. For this purpose, 106 natural landslide dams for which detailed parameters were available have been assembled to provide breach information (Table S1). Dam parameters include debris composition, lake volume and dam height; breach parameters are the peak outflow rate and the breach duration. The breach duration b_d is defined as the period from overflow initiation to dam-breaching termination [29].

As shown in Fig. 12, the peak outflow rate q_b of landslide dams in the field generally increases with dam height h_d and lake volume V_u. q_b is more related to V_u than h_d, indicated by the coefficient of determination R^2. This is because the volume of water released during breaching is directly determined by the lake volume. The effect of the dam height on the peak outflow rate is affected by the lake volume and debris composition. For example, the Shiratani River dam with a height of 190 m had a peak outflow rate of only 580 m^3/s because the dam debris was resistant to erosion [29]. By contrast, the Hsiaolin landslide dam caused by Morakot typhoon had a height of 40 m and the peak outflow rate reached 70649 m^3/s due to a fine-grained debris [20]. In addition, there is no obvious relationship between the breach duration and dam height. This is because the breach duration is affected by the debris composition. Moreover, the breach duration generally increases with the increase of the lake volume.

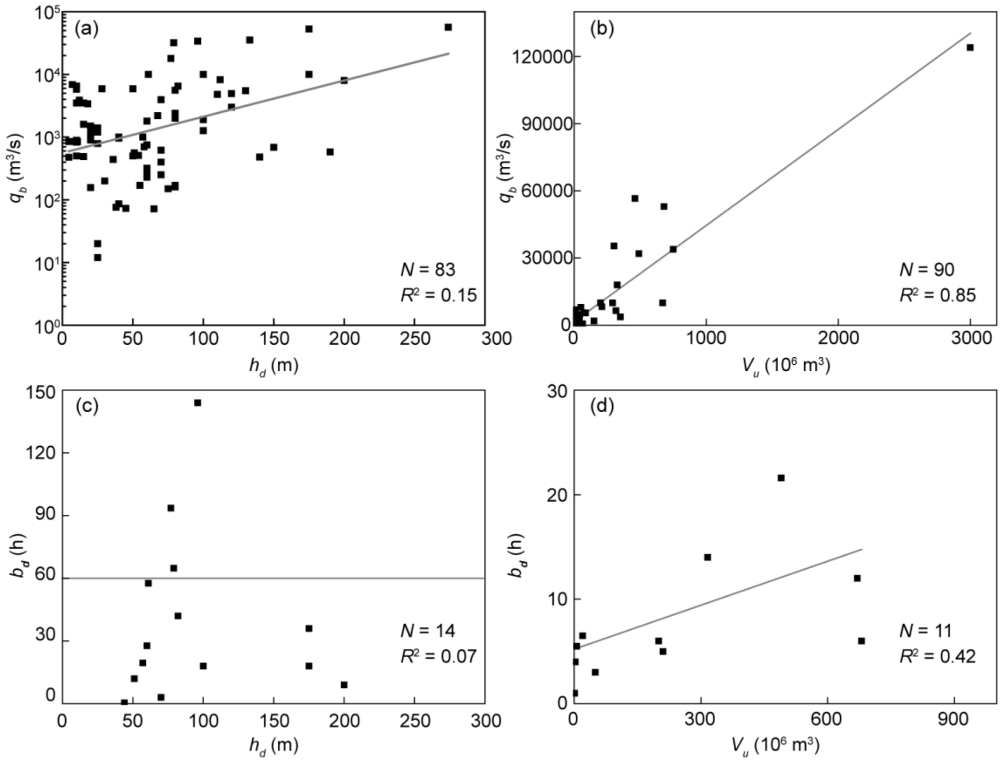

Fig. 12. Relationship between the breach parameters and dam parameters of landslide dams in the field: (a) peak outflow rate q_b and dam height h_d; (b) q_b and lake volume V_u; (c) breach duration b_d and h_d; (d) b_d and V_u. N is the number of landslide dam cases.

The peak outflow rates of tested dams increase with dam height and lake volume. This is in accord with the observations of natural landslide dams (compare Figs. 12 and 13). The quality of regression fit for the tested dams is higher because fine-grained and widely graded dams are considered separately. In addition, compared with the dam height, the peak outflow rate is more related to the breach depth d_b, defined as the difference between dam height and residual dam height. The breach depth is approximately two-thirds of the dam height for fine-grained dams and it is approximately half of the dam height for widely graded dams (Fig. 9). Thus, dam material is incorporated in the correlation between the breach depth and peak outflow rate.

The breach duration of tested dams with the same debris composition increases with increasing dam height (Fig. 13d) in contrast to the tendency for natural landslide dams. This is because the time for breach initiation is significantly affected by the debris composition. For example, the breach initiation time was nearly 72 hours, taking up 80% of the breach duration, for the Tangjiashan landslide dam due to the headcutting migration [5]. By contrast, the breach initiation time was nearly 5 minutes for the Hsiaolin landslide dam composed of fine-grained debris [20]. Furthermore, the breach duration is more relevant to the breach depth than the dam height affected by the debris composition.

The breach duration increases with increasing lake volume, matching field observations. In addition, the slopes of the regressions between the peak outflow rate and dam height as well as peak outflow rate and lake volume are similar for fine-grained and widely graded dams (Figs. 13a and 13c). However, the slopes of the regressions between the breach duration and dam height as well as the breach duration and lake volume are smaller for fine-grained dams than for widely graded dams due to a high shear strength and a low erosion rate (Figs. 13d and 13f).

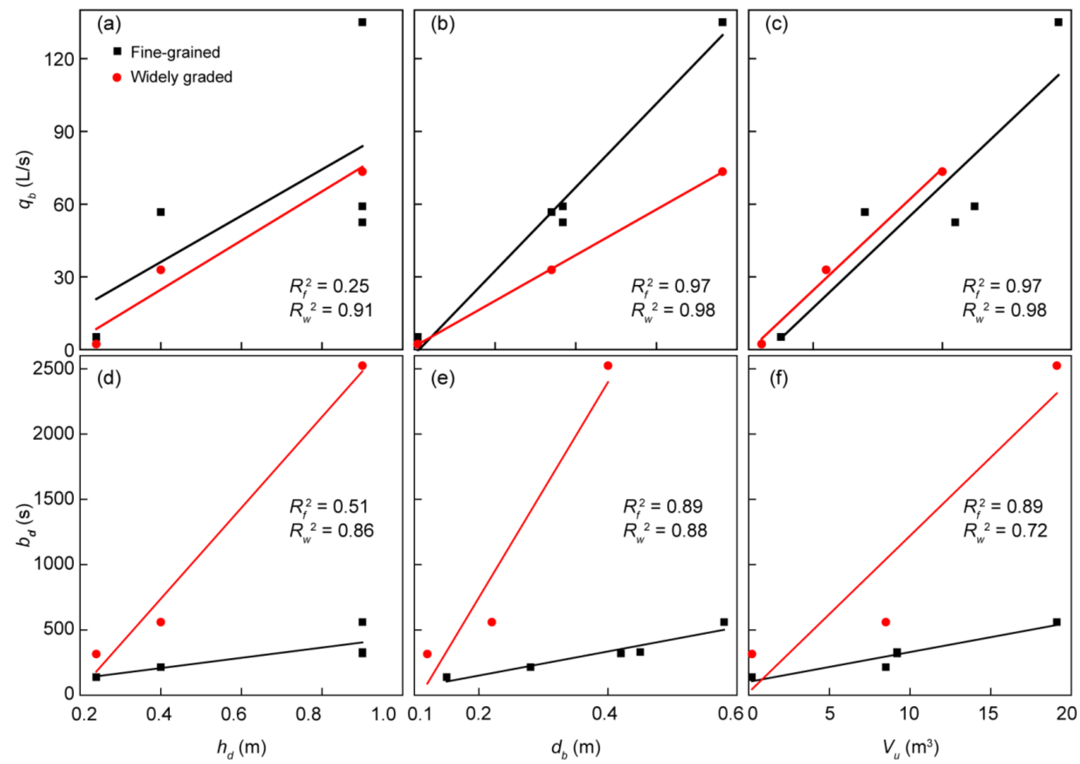

Fig. 13. Relationship between the breach parameters and dam parameters of tested dams: (a) q_b and h_d; (b) q_b and d_b; (c) q_b and V_u; (d) b_d and h_d; (e) b_d and d_b; (f) b_d and V_u. R_f^2 and R_w^2 are the coefficients of determination of fine-grained and widely graded dams, respectively.

4.3 Prediction of peak outflow rate

Regression analysis in a multiplicative form is used to establish an empirical relationship for the peak outflow rate [38]

$$Y = b_0 X_1^{b_1} X_2^{b_2} X_3^{b_3} \tag{5}$$

where Y is the predicted peak discharge and X_i are the control variables described as dam height, lake volume and dam erodibility; e^{α} indicates the erodibility coefficient of the dam [22]; b_i are regression coefficients. An additive form for Equation 5 is expressed through a logarithmic transformation:

$$\text{In}Y = \text{In}b_0 + b_1\text{In}X_1 + b_2\text{In}X_2 + b_3\text{In}X_3 \tag{6}$$

The regression quality is evaluated by the coefficient, R^2,

$$R^2 = 1 - \frac{\sum\left(Y_j - \bar{Y}_j\right)^2}{\sum\left(Y_j - Y_{ave}\right)^2} \tag{7}$$

where Y_{ave} and $\bar{Y}_j$ are the mean value and predicted value of dependent variable Y_i, respectively.

After carrying out the regression analysis of q_b with h_d, V_u, and e^{α}, an equation can be obtained

$$q_b = 910 h_d^{-0.25} V_u^{0.56} e^{\alpha} \tag{8}$$

where α=0 or α=1.38 for the landslide dams with low or high erodibility, respectively. In total, 46 landslide dams with detailed parameters are used for the regression analysis. Widely graded and fine-grained dams in the model tests are regarded as dams with low and high erodibility, respectively, due to significant differences in their erosion rates (Fig. 11). Values of R^2 are 0.82 and 0.97 for landslide dams in the field and in laboratory tests (Fig. 14), respectively, indicating a reasonable prediction. For instance, the 1985 Bairaman landslide dam triggered by the earthquake in Papua New Guinea had a height h_d of 200 m and a lake volume V_u of 5×10^7 m^3 [29]. The debris comprising this landslide dam was highly erodible (highly weathered limestone). The predicted q_b is 8462 m^3/s from Equation 8: close to the recorded estimate (8000 m^3/s). The 2000 Yigong landslide dam induced by the excessive melt water and rainfall had a super peak discharge (q=12400 m^3/s, h_d=60 m, V_u= 3×10^9 m^3) due to large lake volume and high erodibility [28]. The predicted q_b is 113752 m^3/s which matches the observed value.

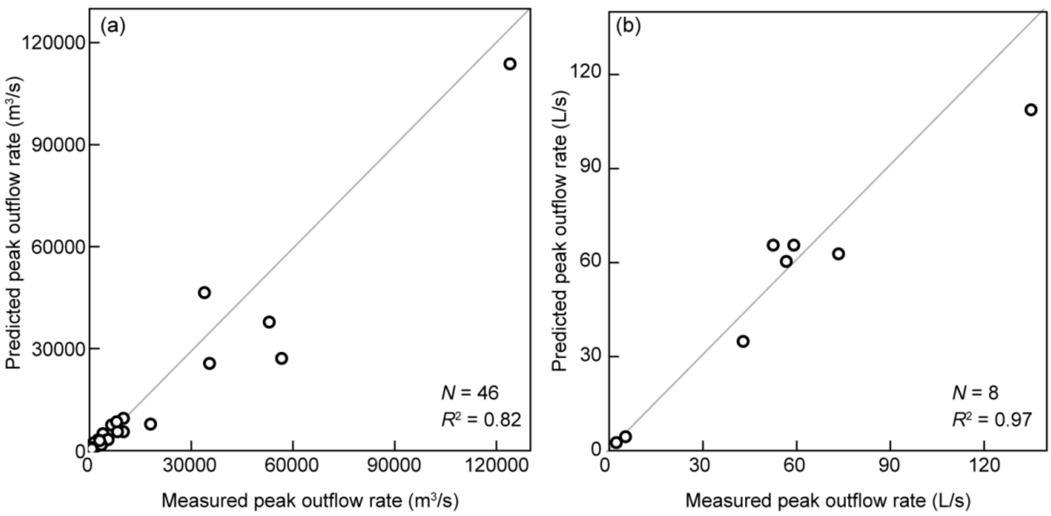

Fig. 14. Comparison between measured and predicted peak outflow rates with the regression analysis: (a) landslide dams in the field; (b) tested dams in this study.

Prediction models of peak discharge based on dam height, lake volume and dam erodibility have been established by Froehlich [14] and Peng and Zhang [22]. Dam erodibility is classified as high, medium or low depending on dam formation, landslide structure and movement distance. Six parameters are included in these prediction models. The evaluation of dam erodibility is complex because detailed dam information is difficult to collect in the short term. Dam erodibility is determined to be low or high based on the grain composition in the model presented here. The prediction accuracy of this simplified model is reasonable as shown in Fig. 14. In addition, coarse-grained dams remain stable and outflow rate is regarded as the inflow rate (Figs. 5 and S4).

5. Discussion

The longitudinal evolution of fine-grained and widely graded dams is first discussed. The slopes of residual dams are then analyzed. Finally, the effects of debris composition and dam height on the peak outflow rate are described.

5.1 Longitudinal evolution of landslide dams

For dams in tests F1–F5, the downstream slope angle above the phreatic line quickly decreased when the dam debris was entrained downstream by the outburst flood (Figs. 15a and S7). A flat angle varying from 14.4–17.2° was then maintained in the breach process. This longitudinal evolution of fine-grained dams is in agreement with the theoretical model presented by Powledge et al. [24]. This model assumes that the downstream slope angle quickly varies until a constant angle of critical soil friction is reached, after which this slope angle is kept to the dam-breaching end [24]. However, the φ value (26.8°) of fine-grained debris is larger than the constant slope angle for the dams according to the equilibrium of energy loss. This is because the influence of seepage on the dam slope is not incorporated in the theoretical model. Based on an equilibrium analysis with Equations 1–4, the slope angle of a fine-grained dam is about 15° when the hydraulic gradient increases to 0.35 before overtopping (Fig. 6). This slope angle matches the values of the longitudinal slope during breaching.

A cascading-step structure is formed for widely graded dams (Figs. 15b and S8) which is in accordance with the observation of the Tangjiashan dam [5]. However, it does not occur for fine-grained dams. The critical velocity v_c for debris movement of the material dominated by sand and gravel was estimated by Briaud [3]:

$$v_c = 0.35\left(d_{50}\right)^{0.45} \tag{9}$$

v_c values are 0.3 m/s and 0.6 m/s for fine-grained and widely graded debris, respectively. The flow velocities u of fine-grained and widely graded dams during the breach process are 0.1–1.1 m/s and 0.1–0.7 m/s, respectively, calculated by the outflow rate and water depth. Fine-grained debris is apt to be washed away and headcutting is not developed because of a significant difference between u and v_c. By contrast, fines in a widely graded dam are first carried away and leave coarse gravel behind due to the limited flow velocity. Coarse gravel without surrounding fines is then entrained by the outburst flood.

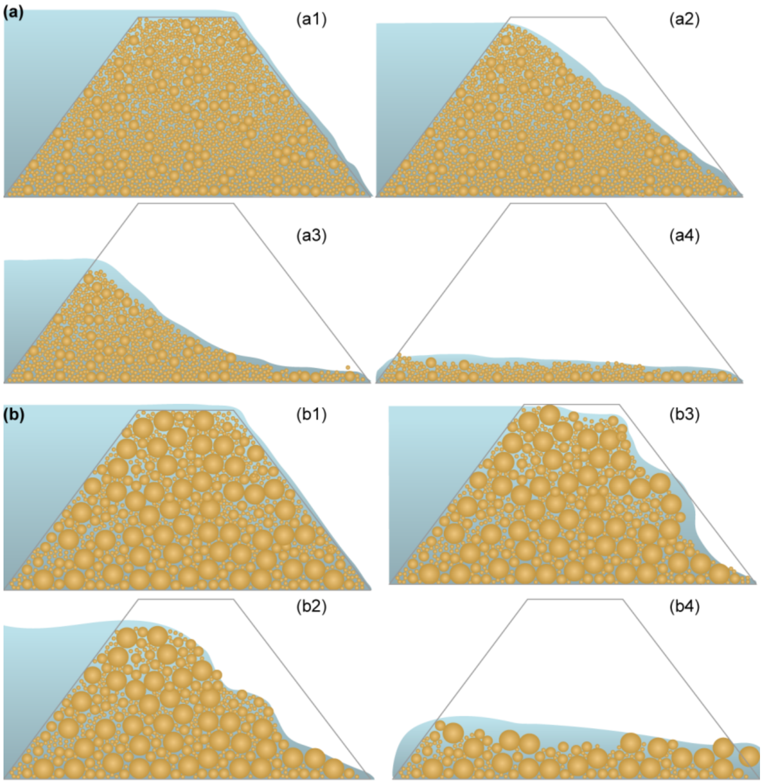

Fig. 15. Longitudinal evolution of landslide dams during breach: (a) fine-grained dams; (b) widely graded dams.

Piping did not develop for all tested dams, although the fine debris at the toe of the dams in tests W1–W3 and C1–C3 was carried away by the seepage. This is consistent with field observations that only 8% of landslide dams fail by piping [40, 22]. The corresponding value for man-made rockfill and earth dams is up to 37%. The reason is the widths of landslide dams are usually large and piping channels are not completely formed before overtopping. In addition, landslide dam debris is weakly sorted and the dams remain internally stable. According to stability criteria provided by Chang and Zhang [6], debris material with less than 5% fines content is internally stable when $(H/F)_{min} > 1.0$ is satisfied where F is the mass fraction of debris smaller than grain diameter d, and H is the mass fraction of debris within the range d–$4d$. Based on this criterion, fine-grained and widely graded dams are stable under seepage and coarse-grained dams are unstable (Fig. 2). However, coarse-grained dams in our tests are stable due to the skeletal support effect of the coarse grains. The effective stress of the dams exists although local seepage failure may develop in the dam body. This process has been simulated by coupled discrete element method and computational fluid dynamics [31].

5.2 Residual dams

Compared with rockfill and earth dams, the final breach of landslide dams often cannot reach the original river bed and incomplete erosion is likely to occur. This is because the widths and volumes of landslide dams are larger and the dams can't be completely carried away. In addition, coarse cobbles may be present at the bottom or side walls of the breach of landslide dams because of their heterogeneity [44]. These cobbles inhibit the undercut of the breach by the outburst flood.

In general, slope angles of residual dams are higher than the longitudinal gradient of the river (Fig. 16). The residual dams can be gradually carried downstream by the seasonal flood and the deposition thickness is lowered accordingly [37].

However, the residual dams may breach again when the breach is blocked. For example, the residual dam of the Tangjiashan landslide dam was blocked by the debris flow in the Dashui gully on 24 September 2008 and the water depth of the backwater lake increased by 8 m [15]. The breach was again undercut and broadened by the overtopping flow. The Baige landslide dam with a height of 61 m failed by overtopping on 11 October 2018. The peak outflow rate was 10000 m^3/s and the breach depth was 32 m. Subsequently, the breach was blocked by a second landslide on 3 November 2018 and the dam height increased to 96 m. The dam failed again with a peak outflow rate of 33900 m^3/s and a depth of 61 m [40].

The slope angle θ of residual dams in the stream direction decreases first with dam height and then increases (Fig. 16). This is because the lake shape coefficients of the dams with heights of 0.40 m were higher than those of the other dams (Table 2). In addition, the slope angle and deposition thickness of residual dams composed of fine-grained debris are smaller than those of widely graded dams (Figs. 9 and 16). The potential breach risk caused by residual dams composed of widely graded debris is larger, although their peak outflow rates during breach are smaller.

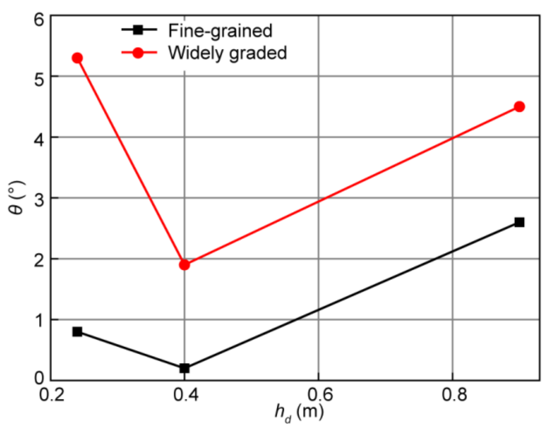

Fig. 16. Relationship between the dam height h_d and slope angle θ of the residual dam in tests F1–F3 and W1–W3. Regardless of the dam height, the slope angles of fine-grained dams are smaller than those of widely graded dams.

5.3 Effects of debris composition and dam height on the peak outflow rates

Peak outflow rates of landslide dams increase with increasing dam height (Figs. 12a and 13a). However, lake volume is more closely related to the peak outflow rate (Figs. 12b and 13c). Since the dam height is related to the lake volume, only the lake volume was used by Costa and Schuster [11] in an empirical equation for estimating the peak outflow rate. Our tests also show that peak outflow rate for the fine-grained dam in test F2 matches the values in tests F4 and F5 due to the same lake volumes (Fig. 10).

Peak outflow rates of landslide dams are significantly affected by the debris gradation. Peak outflow rates of widely graded dams were 0.4–0.6 times those of fine-grained dams with the same dam height (Fig. 10). The breach depths of fine-grained dams are two-thirds of the dam height compared to half the dam height for widely graded dams (Fig. 9). The debris composition of landslide dams can be rapidly assessed by remote sensing images with high precision [40]. As a result, peak outflow rates of landslide dams can be further predicted by physically based numerical models like DABA [30] if the breach depth is estimated. Furthermore, the peak outflow rate can be estimated from the regression analysis of the dam height, lake volume and erodibility coefficient using Equations 5–8.

5.4 Implications and limitations

The armoring layer in Fig. 8 is termed a 'boulder bar' by Jiang et al. [16]. The boulder bar was formed after peak discharge because the breach discharge gradually reduced. This bar first occurred near the dam toe and then gradually extended in the stream direction. These phenomena are consistent with the observations of laboratory tests and the Yigong and Tangjiashan dams in the field [16, 36]. It shows that the results are credible and can provide a reference for the evolution of river morphology.

The effect of river bed slope θ_b on dam failure is not considered in this research. Dams with d_{50}=0.85 mm, θ_b = 12° fail by overtopping as indicated by Zhou et al. [45]; this is in line with the failure mode of fine-grained dams with d_{50}=0.80 mm presented here. Dams with fine sand fail by overtopping to the slope failure and then overtopping with the increase of the bed slope by Jiang et al. [18]. The sliding stress is increased in Eq. (2) by an increase in channel bed slope and thus results in the slope failure of dam downstream: similar to the seepage instability of fine-grained dams. Our experimental results are applicable to landslide dams with a gentle river slope.

6. Conclusions

We experimentally analyzed the failure processes of landslide dams by varying debris composition and geomorphic parameters (dam height and lake volume). In particular, we identified the failure mode and predicted peak outflow rates based on 106 landslide dams in the field and model tests.

(1) The failure modes of landslide dams were regulated by the shear strength and seepage. Fine-grained dams failed by overtopping along with seepage instability and widely graded dams failed by headcutting. However, coarse-grained dams remained

stable, regardless of the dam height or lake volume. Affected by the seepage, a flat angle was maintained in the longitudinal section during breaching of fine-grained dams. By contrast, a cascading-step structure was formed for the widely graded dams.

(2) The time for breach initiation of fine-grained dams is nearly the same for different dam heights due to slope failure caused by seepage. By contrast, the initiation time for widely graded dams significantly increased with increasing dam height. The breach durations of fine-grained dams were significantly shorter than those of widely graded dams because of headcutting migration and a low erosion rate for widely graded debris. The peak outflow rate and breach duration were more closely related to the breach depth than the dam height because the debris composition was considered in the former.

(3) Lake volume was more relevant to the peak outflow rate than the dam height. The peak outflow rate can be reasonably predicted by a regression analysis with the dam height, lake volume and debris composition.

(4) Debris grains were uniformly distributed for fine-grained dams after breaching but an armoring layer formed on the surface of widely graded dams due to grain segregation. The slope angle of residual dams in the stream direction decreased first with dam height and then increased, affected by the lake shape coefficient. In addition, the slope angle and thickness of residual dams composed of fine-grained debris were smaller than those of widely graded dams.

The test results show that the breach process and failure mode of landslide dams is regulated by the interaction between the dam and the backwater lake, posing a challenge to predict the peak discharge. The effect of river bed slope on the landslide dam failure will be considered in further research.

Acknowledgements

We acknowledge funding from the Natural Science Foundation of China (No. 42007252). Constructive reviews by the editor and two anonymous reviewers helped to improve the manuscript and are gratefully acknowledged.

Conflicts of Interests

The authors declare that they do not have any conflict of interest.

Notation

b_d	breach duration of a dam
b_l	length of backwater lake
c	cohesion of dam material
c_d	dam shape coefficient
c_l	lake shape coefficient
C_c	curvature coefficient of the grading curve
C_u	uniformity coefficient of the grading curve
d	grain size
d_{50}	median grain size of a dam material
E	mean erosion rate of a dam
f_s	seepage stress
F_s	sliding stress generated by gravity
g	gravitational acceleration

G_s specific gravity

h slide thickness

h_d dam height

h_r the maximum residual dam height

h_u upstream water level

h_w water depth

i hydraulic gradient

k saturated permeability coefficient of dam material

l_d length of residual dam

q_b peak outflow rate of a dam

R_s resistance stress

R^2 coefficient of determination

s stability coefficient of a downstream dam slope

v_c critical velocity for grain initiation

V_u volume of backwater lake

α angle of downstream dam slope

θ slope angle of a residual dam

θ_b slope angle of a river bed

ρ_d dry density of a dam material

ρ_s grain density

ρ_w water density

σ effective normal stress

φ internal friction angle of a dam material

γ_w unit weight of water

References

1. Annandale GW (2006) Scour technology-mechanics and engineering practice. McGraw-Hill, New York, p 430.
2. Awal R, Nakagawa H, Kawaike K, Baba Y, Zhang H (2008). Prediction of Flood/Debris Flow Hydrograph due to Landslide Dam Failure by Overtopping and Sliding. Annuals of Disaster Prevention Research Institute, Kyoto University 51(B), pp. 603–611.
3. Briaud J (2008) Case Histories in Soil and Rock Erosion: Woodrow Wilson Bridge, Brazos River Meander, Normandy Cliffs, and New Orleans Levees. J. Geotech. Geoenviron. Eng 134(10): 1425–1447.
4. Canuti P, Casagli N, Ermini L (1998) Inventory of landslide dams in the Northern Apennine as a model for induced flood hazard forecasting. Managing Hydro-Geological Disasters in a Vulnerable Environment. CNR-GNDCI and UNESCO IHP, Perugia, 189–202.
5. Chang DS, Zhang LM (2010) Simulation of the erosion process of landslide dams due to overtopping considering variations in soil erodibility along depth. Nat. Hazards Earth Syst. Sci 10(4): 933–946.
6. Chang DS, Zhang LM (2013) Extended internal stability criteria for soils under seepage. Soils Found 53(4): 569–583.
7. Chanson H (2015) Embankment overtopping protection systems. Acta Geotech. 10: 305–318.
8. Chen KT, Chen TC, Chen XQ, Chen HY, Zhao, WY (2021) An experimental determination of the relationship between the minimum height of landslide dams and the run-out distance of landslides. Landslides 18: 2111–2124.

9. Chen SC, Lin TW, Chen CY (2015) Modeling of natural dam failure modes and downstream riverbed morphological changes with different dam materials in a flume test. Eng. Geol 188: 148–158.

10. Chen S, Chen Z, Tao R, Yu S, Xu W, Zhou X, Zhou Z (2018) Emergency response and back analysis of the failures of earthquake triggered cascade landslide dams on the Mianyuan River, China. Nat. Hazards Rev 19(3): 05018005.

11. Costa JE, Schuster RL (1991) Documented historical landslide dams from around the world. U.S. Geological Survey Open-File Report , 91–239.

12. Ermini L, Casagli N (2003) Prediction of the behaviour of landslide dams using a geomorphological dimensionless index. Earth Surf. Process. Landf 28(1): 31–47.

13. Fan X, Dufresne A, Subramanian S, Strom A, Hermanns R, Stefanellif C et al (2020) The formation and impact of landslide dams – State of the art. Earth-Sci. Rev 203: 103116.

14. Froehlich D C (2022). Peak flood discharge from a landslide dam outburst. Nat. Hazards Rev 23(2): 04022001.

15. Hu X, Lv X, Huang R, Ren X, Wang X, Liu J (2009) Analyses of river-blocking and breaking mode of "9·24" debris flow near Tangjiashan barrier dam. Journal of Southwest Jiaotong University, 44(3), 312–326 (in Chinese).

16. Jiang X, Cheng H, Gao L, Liu W (2021) The formation and geometry characteristics of boulder bars due to outburst floods triggered by overtopped landslide dam failure. Earth Surf. Dyn 9(5): 1263–1277.

17. Jiang X, Huang J, Wei Y, Niu Z, Chen F, Zou Z, Zhu Z (2018) The influence of materials on the breaching process of natural dams. Landslides, 2018, 15: 243-255.

18. Jiang X, Wei Y, Wu L, Lei Y (2018) Experimental investigation of failure modes and breaching characteristics of natural dams. Geomatics, Natural Hazards and Risk, 9(1): 33–48.

19. Korup O (2004) Geomorphometric characteristics of New Zealand landslide dams. Eng. Geol 73: 13–35.

20. Li MH, et al (2011) The formation and breaching of a short-lived landslide dam at Hsiaolin Village, Taiwan—Part II: Simulation of debris flow with landslide dam breach. Eng. Geol 123: 60–71.

21. Neill CR (1973) Guide to bridge hydraulics. University of Toronto Press, Toronto, p 191.

22. Peng M, Zhang LM (2012) Breaching parameters of landslide dams. Landslides 9(1): 13–31.

23. Peng M et al (2014) Engineering risk mitigation measures for the landslide dams induced by the 2008 Wenchuan earthquake. Eng Geol 180: 68–84.

24. Powledge GR et al (1989) Mechanics of overflow erosion on embankments, II: hydraulic and design considerations. J Hydraul Eng 115 (8): 1056–1075.

25. Risley J, Walder J, Denlinger R (2006) Usoi dam wave overtopping and flood routing in the Bartang and Panj Rivers,Tajikistan. Nat. Hazards 38: 375–390.

26. Ruan HC, Chen HY, Li Y, Chen JG, Li HB (2021) Study on the downcutting rate of a debris flow dam based on grain-size distribution. Geomorphology 391: 107891.

27. Shan Y, Chen S, Zhong Q (2020) Rapid prediction of landslide dam stability using the logistic regression method. Landslides 17: 2931–2956.

28. Shang YJ, Yang ZF, Li LH, Liu DA, Liao QL, Wang YC (2003) A super-large landslide in Tibet in 2000: background, occurrence, disaster, and origin. Geomorphology 54(3–4): 225–243.

29. Shen DY, Shi ZM, Peng M, Zhang LM, Jiang MZ (2020) Longevity analysis of landslide dams. Landslides 17(8): 1797–1821.

30. Shi ZM, Guan SG, Peng M, Zhang LM, Zhu Y, Cai QP (2015) Cascading breaching of the Tangjiashan landslide dam and two smaller downstream landslide dams. Eng. Geol 193: 445–458.

31. Shi ZM, Zheng, HC, Yu, SB, Peng, M, Jiang, T (2018) Application of CFD-DEM to investigate seepage characteristics of landslide dam materials. Comput. Geotech 101: 23–33.

32. GB50123-2019, Standard of geotechnical testing method (in Chinese).

33. Stefanelli CT, Segoni S, Casagli N, Catani F, (2016) Geomorphic indexing of landslide dams evolution. Eng. Geol. 208: 1–10.

34. Wang Z, Melching CS, Duan X, Yu G (2012) Stability of landslide dams and development of knickpoints. Environ Earth Sci. 65(4): 1067–1080.

35. Wang Z et al (2009) Ecological and hydraulic studies of step-pool systems. J Hydraul Eng. 135(9): 705–717.

36. Wu CH, Hu KH, Liu WM, Wang H, Hu XD, Zhang XP, (2020) Morpho-sedimentary and stratigraphic characteristics of the 2000 Yigong River landslide dam outburst flood deposits eastern Tibetan Plateau. Geomorphology 367: 107293.

37. Xiong J, Tang C, Gong L, Chen M, Li N, Shi Q, Zhang X, Chang M, Li M (2022) How landslide sediments are transferred out of an alpine basin: Evidence from the epicentre of the Wenchuan earthquake. Catena 208: 105781.

38. Xu Y, Zhang L (2009) Breaching parameters for earth and rockfill dams. J. Geotech. Geoenviron. Eng 135(12): 1957–1970.

39. Yang E, Bui HH, Nguyen GD. et al. (2021) Numerical investigation of the mechanism of granular flow impact on rigid control structures. Acta Geotechnica 16: 2505–2527.

40. Zhang LM, Xiao T, He J, Chen C (2019) Erosion-based analysis of breaching of Baige landslide dams on the Jinsha river, China, in 2018. Landslides 16(10): 1965–1979.

41. Zheng H, Shi Z, Shen D, Peng M, Hanley KJ, Ma C, Zhang, L (2021a) Recent advances in stability and failure mechanisms of landslide dams. Front. Earth Sci 9: 659935.

42. Zheng H, Shi Z, Yu S, Fan X, Hanley KJ, Feng S (2021b) Erosion mechanisms of debris flow on the sediment bed. Water Resour. Res. 57 (12): WR030707.

43. Zheng H, Shi Z, Peng M, Guan S, Hanley KJ, Feng S (2021c) Amplification effect of cascading breach discharge of landslide dams. Landslides 195.

44. Zhong QM, Chen SS, Mei SA, Cao W, (2018) Numerical simulation of landslide dam breaching due to overtopping. Landslides 15(6): 1183–1192.

45. Zhou GGD, Zhou M, Shrestha MS, Song D, Choi CE, Cui K, Peng M, Shi Z, Zhu X, Chen H, (2019) Experimental investigation on the longitudinal evolution of landslide dam breaching and outburst floods. Geomorphology 334: 29–43.

46. Zhu XH, Peng JB, Liu BX, Jiang C, Guo J (2020) Influence of textural properties on the failure mode and process of landslide dams. Eng. Geol. 271: 105613.

Supplementary Information for "Effects of soil properties and geomorphic parameters on the breach mechanisms of landslide dams and prediction of peak discharge"

Shenggong Guan[1], Zhenming Shi[1], Hongchao Zheng[1]*, Danyi Shen[1], Kevin J Hanley[2], Jiangtao Yang[1], Chengzhi Xia[1]

[1]Department of Geotechnical Engineering, College of Civil Engineering, Tongji University, China

[2]School of Engineering, Institute for Infrastructure and Environment, The University of Edinburgh, United Kingdom

Contents:

Table S1: Landslide dams used for analysis (106 cases)

Fig. S1. Experimental dam debris in various components

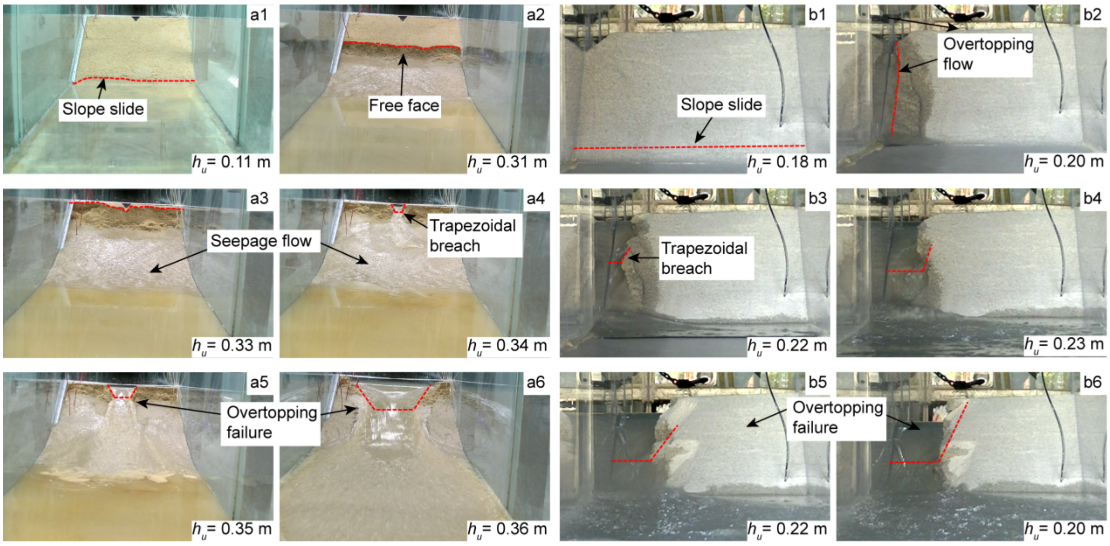

Fig. S2. Breach processes of the fine-grained dams in tests F2 and F3. These processes were similar to those of test F1 in Fig. 3.

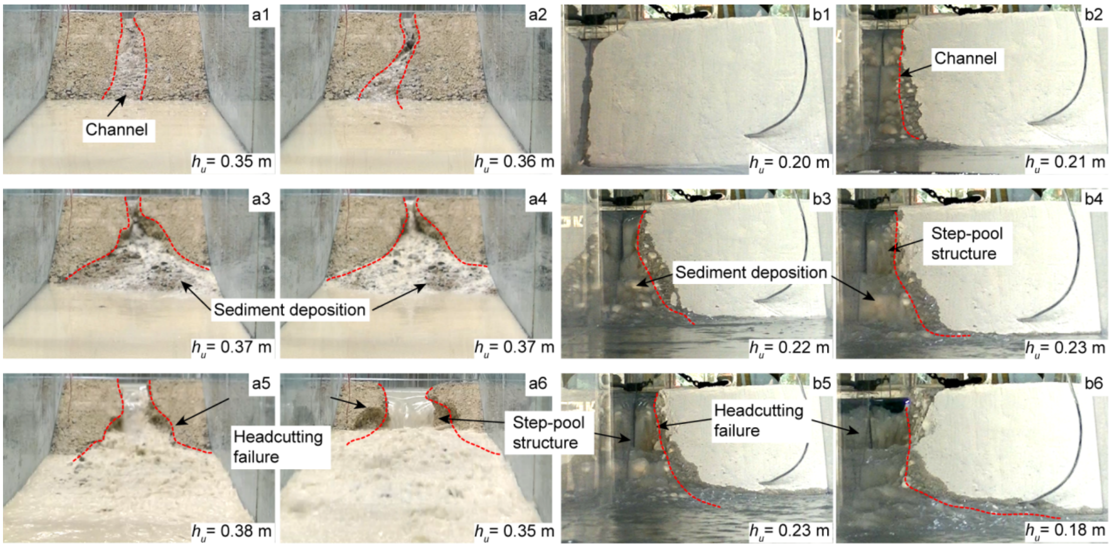

Fig. S3. Breach processes of the widely graded dams in tests W2 and W3. These processes were similar to those of test W1 in Fig. 4.

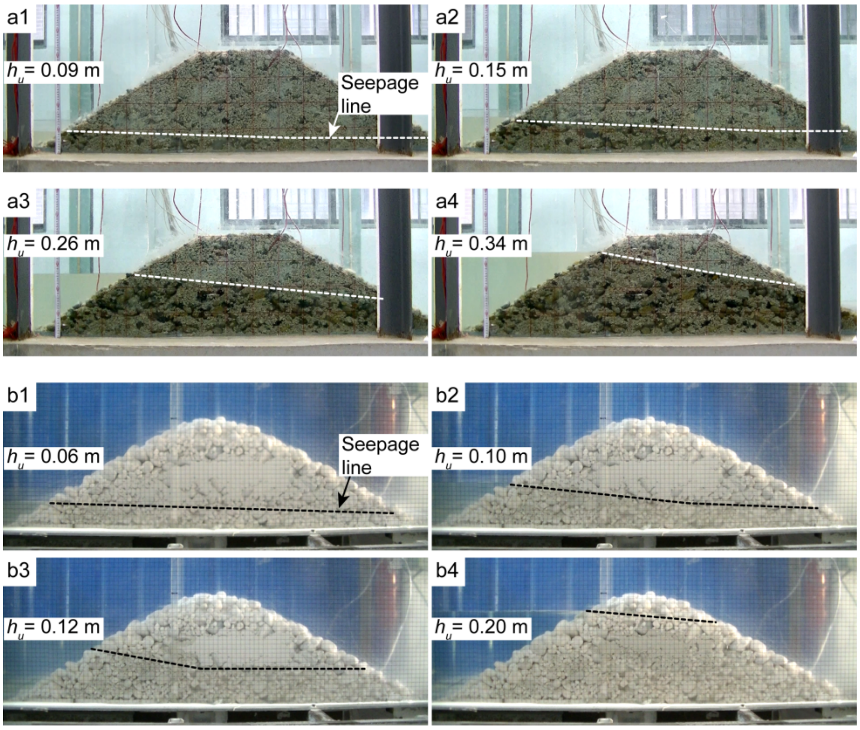

Fig. S4. Stability of dams with coarse-grained debris in tests C2 and C3. These processes were similar to those of test C1 in Fig. 5.

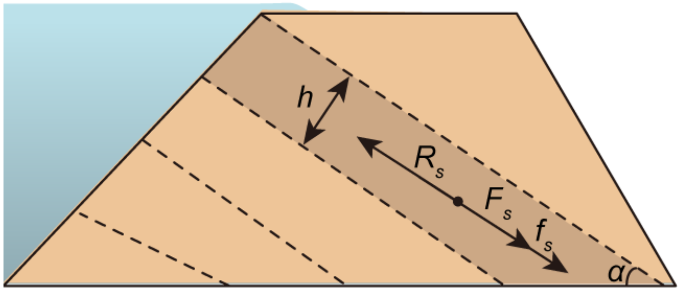

Fig. S5. Stability analysis of seepage stress on a dam downstream. *h* is the slide depth, α is the slope angle, F_s is the sliding stress generated by gravity, R_s is the resistance stress and f_s is the seepage stress. The shear stress exerted by the breach flood is not considered for a simplified calculation.

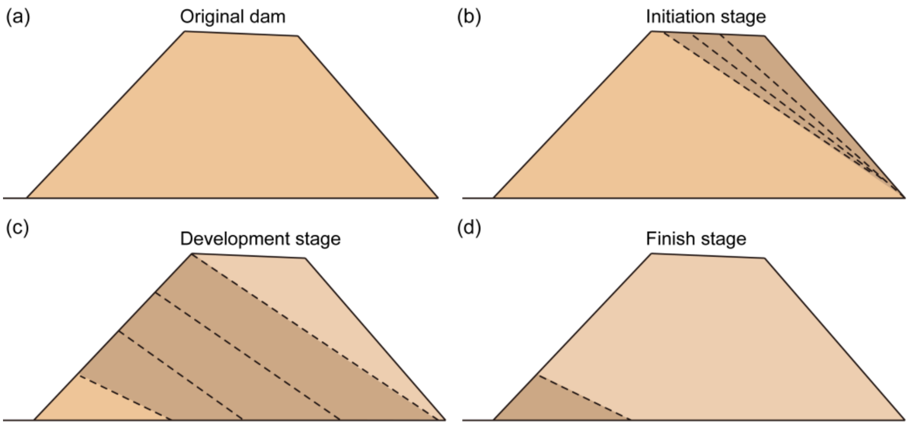

Fig. S6. Breach development of a landslide dam: (a) original dam; (b) initiation stage; (c) development stage; (d) finish stage.

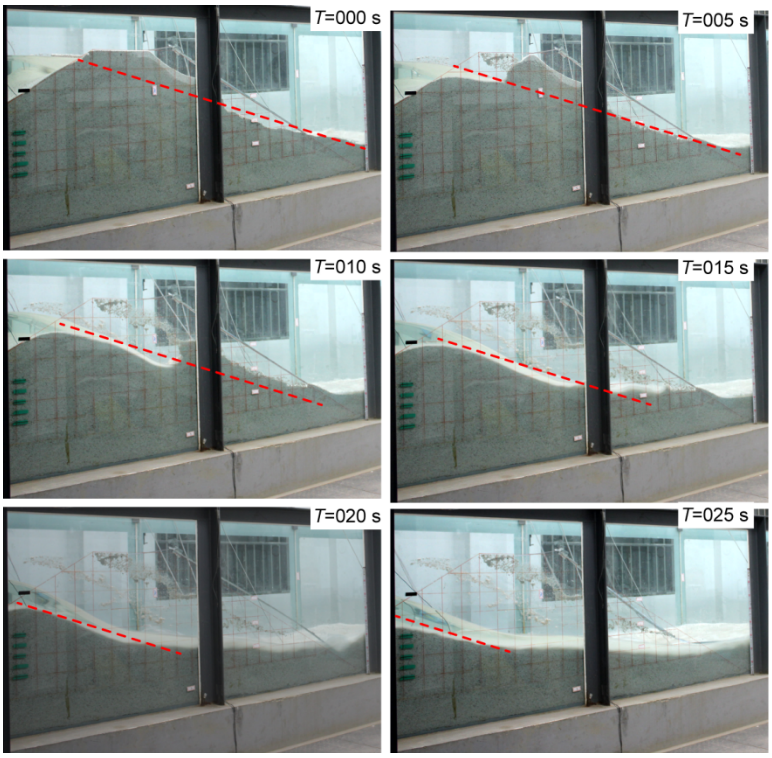

Fig. S7. Longitudinal evolution of the landslide dam during breaching in test F1. *T* is the time elapsed from the first picture. The definition of *T* is the same for the following Fig. S8. A flat angle was maintained for fine-grained dams during breaching.

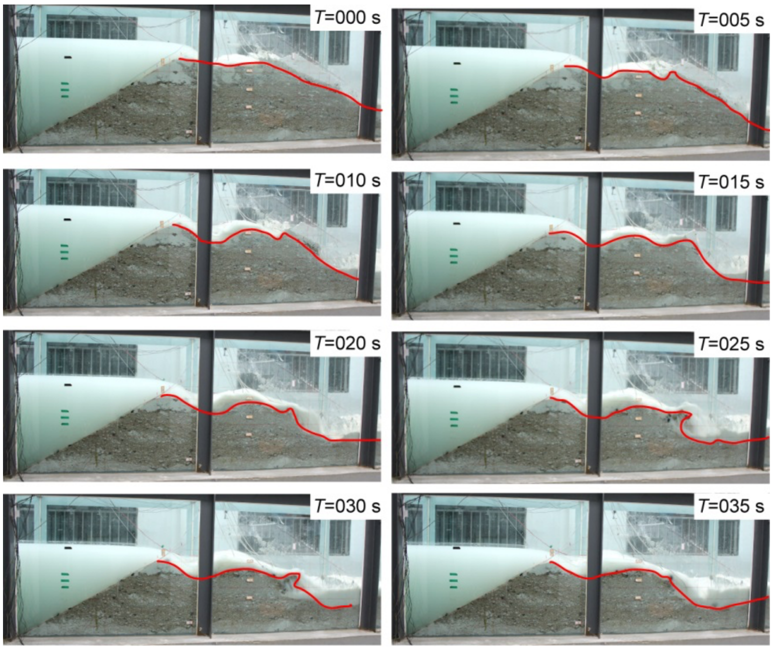

Fig. S8. Longitudinal evolution of the landslide dam during breaching in test W1. A step-pool structure was developed for widely graded dams.

Table S1 Landslide dams used for analysis (106 cases)

Number	Name	Region	Time	h_d (m)	d_w (m)	V_d (10^6 m^3)	V_u (10^6 m^3)	e	b_d (h)	q_b (m^3/s)
1	Donghekou	CN	2008	20	750	12	6	L	-	800~1000
2	Fengmingqiao	CN	2008	10	300	0.14	1.8	L	-	500
3	Hongshi River	CN	2008	50	500	18	4	L	-	400~600
4	Jiadanwan	CN	2008	60	220	8.2	6.1	L	-	-
5	Jiaozigou	CN	2008	60	250	1.8	6.2	L	-	-
6	Liudinggou	CN	2008	60	500	1.5	3	L	-	-
7	Maanshi	CN	2008	67.6	275	5.8	1.15	H	-	2200
8	Miduigou	CN	1988	100	20	-	1.95	H	-	1270
9	Muguaping	CN	2008	15	20	0.2	0.04	H	-	-
10	Shibangou	CN	2008	30	800	15	11	L	-	-

11	Tanggudong	CN	1967	175	3000	68	680	H	6	53000
12	Tangjiashan	CN	2008	82	611.8	20.37	316	L	14	6500
13	Xiaogangjian	CN	2008	70	300	2	12	H	-	3950
14	Xiaojiaqiao	CN	2008	57	200	2.42	20	L	6.5	1000
15	Yanziyan	CN	2008	10	20	0.006	0.03	H	-	-
16	Yibadao	CN	2008	25	140~180	0.15	3.79	L	-	-
17	Yigong	CN	2000	60	2200~2500	300	3000	H	9.25	124000
18	Zhebozu	CN	1965	51	650	29	2.7	L	4	560
19	Xiaolincun	TW	2009	44	1500	15.4	9.9	-	0.14	70649
20	Longquanxi	TW	2006	40	64	0.6	1	L	-	-
21	Tamari Creek	TW	2009	10	1200	-	5.33	H	-	-
22	Tsatichuu	Bhutan	2003	110	700	5	1.5	H	-	-
23	Rio Toro River	Costa	1992	70	600	3	0.5	L	-	400

		Rica								
24	La Josefina	Ecuador	1993	100	1100	20	200	L	6	10000
25	Pisque	Ecuador	1990	58	450	1	2.5	L	-	700
26	Rio Paute	Ecuador	1993	112	800	25	210	L	4~6	8250
27	Birehi Ganga	India	1893	274	2750	286	460	H	-	56650
28	Buonamico	Italy	1973	90	700	21	7.5	H	-	-
29	Tegermach (Lake Yashinkul)	Soviet Union	1835	120	60	20	6.6	H	-	4960
30	Mantaro	Peru	1945	133	580	3.5	301	H	-	35400
31	Mantaro	Peru	1974	175	3800	1300	670	L	12	10000
32	Bairaman	Papua New Guinea	1985	200	3000	200	50	H	3	8000

33	Karli stream	Pakistan	2005	130	450	-	86	L	-	5500
34	Tunawaea	NZ	1991	70	550	4	0.9	L	1	250
35	Mt. Adams	NZ	1999	80~100	700	10~15	5~7	H	5.5	2000~3000
36	Ram Creek	NZ	1968	40	1200	2.8	1.1	-	-	1000
37	Cedar Creek	America	1988	3	150	1.7	0.053	H	-	-
38	East Fork Hood River	America	1980	10.7	225	0.07~01	0.105	-	-	850
39	Gros Ventre River	America	1925	70	3000	-	80	L	-	-
40	Jackson Creek Lake	America	1980	4.5	180	0.77	2.47	L	-	477
41	Wyoming	America	1925	70~75	30000	38	80	L	-	-
42	Jishixia	CN	8000BP	200	1500	45	11.71	-	-	8.71
43	Arida	JP	1953	10	150	0.18	0.047	L	-	890
44	Arida	JP	1953	60	500	2.6	17	L	-	750
45	Asahi	JP	1889	25	300	0.45	0.92	L	-	790

46	Azusa	JP	1915	4.5	600	0.9	0.53	-	-	850
47	Azusa	JP	1926	10	330	2	1.2	-	-	850
48	Banjo	JP	1943	80	250	1.5	14	-	-	160
49	Hime	JP	1911	60	500	1.9	16	L	-	1800
50	Iketsu	JP	1889	140	180	3.4	26	L	-	480
51	Imanishi	JP	1889	60	250	1.1	6.4	-	-	230
52	Imanishi	JP	1889	75	125	1.1	9	-	-	150
53	Kaifu	JP	1892	45	350	2	14	-	-	73
54	Kaminirau	JP	1788	36	500	2	2.2	-	-	440
55	Kano	JP	1889	15	130	0.094	1.3	H	-	1600
56	Kano	JP	1889	20	120	0.1	0.6	-	-	1300
57	Kano	JP	1889	20	100	0.15	1	H	-	1500
58	Kano	JP	1889	25	200	0.44	1.8	H	-	1400

59	Kawarabitsu	JP	1889	80	700	13	40	-	-	2000
60	Koshibu	JP	1961	6	800	2.4	0.4	-	-	850
61	Matsu	JP	1891	55	230	3.2	3.1	-	-	170
62	Nakaya	JP	1953	40	200	0.4	0.27	-	-	86
63	Nishi	JP	1889	20	250	0.6	1.3	L	-	980
64	Nishi	JP	1889	20	120	0.63	0.4	H	-	1100
65	Nishi	JP	1889	25	250	0.63	1.8	H	-	1200
66	Nishi	JP	1889	25	250	0.93	0.11	-	-	20
67	Niu	JP	1982	15	150	0.18	1.3	L	-	490
68	Oi	JP	1889	100	150	2.6	2.3	-	-	10
69	Ojika	JP	1683	70	400	3.3	64	-	-	620
70	Oshiro	JP	1586	60	300	1.2	6.4	L	-	270
71	Oshiro	JP	1586	60	250	1	6	L	-	320

72	Sai	JP	1847	65-100	650	21	350	-	-	3700
73	Sakauchi	JP	1895	38	350	0.96	2	-	-	76
74	Shinsei	JP	1923	10	200	0.18	0.037	-	-	2
75	Shiratani	JP	1889	190	500	10	38	-	-	580
76	Shiratani	JP	1953	25	100	0.09	0.06	-	-	12
77	Sho River	JP	1586	100	600	19	150	-	-	1900
78	Susobana	JP	1847	54	300	1.2	16	-	-	510
79	Totsu	JP	1889	18	450	0.036	0.78	-	-	3400
80	Totsu	JP	1889	7	250	0.073	0.65	-	-	6900
81	Totsu	JP	1889	10	150	0.15	0.56	-	-	5800
82	Totsu	JP	1889	10	380	0.23	0.93	-	-	3500
83	Totsu	JP	1889	80	350	2.5	17	L	-	2400
84	Totsu	JP	1889	110	690	3.1	42	-	-	4800

85	Totsu	JP	1889	50	300	0.85	1.6	-	-	5900
86	Totsu	JP	1889	28	500	1.7	3.2	-	-	5900
87	Totsu	JP	1889	10	220	0.28	0.52	-	-	6500
88	Totsu	JP	1889	12	250	0.27	0.72	-	-	3900
89	Yamate	JP	1889	80	350	4.2	12	-	-	170
90	Yanagikubo	JP	1847	35	250	0.65	1.4	-	-	24
91	Nagano Prefecture	JP	1984	40	3300	26	3.7	L	-	960
92	Deshanbaigu	JP	1965	65	260	0.98	2	L	-	72
93	Yoda kawawa	JP	1953	10	80	0.017	0.03	-	-	830
94	Tegermach	USSR	1835	120	60	20	6.6	-	-	4960
95	Nakawa	JP	1892	80	330	3.3	75	-	-	5600
96	Torn	JP	1858	150	200	0.4	3.8	L	-	687
97	Torn	JP	1858	20	700	12	4.1	-	-	157

98	Dahechuan	JP	1932	15	170	0.91	10	L	-	3500
99	Houei	JP	1707	30	650	4	4.7	-	-	200
100	Shijinchuan	JP	1889	20	300	0.6	1.3	-	-	980
101	Baige#1(Jinsha River)	CN	2018	61	3000	22	290	-	19.2	10000
102	Poerua	NZ	1999	120	700	12.5	6	H	-	3000
103	hongsong	CN	2008	37	100	0.26	1	-	-	0.5
104	Jiala#1(yaluzangbujiang)	CN	2018	79	2400	50	490	-	21.6	32000
105	Baige#2(Jinsha River)	CN	2018	96	580	30.2	750	H	48	33900
106	Jiala#2(yaluzangbujiang)	CN	2018	77	3500	30	326	L	31.2	18000

Note: CN = China, NZ = New Zealand, JP = Japan, TW = Taiwan, L = Low, H = High.

h_d and d_w are the dam height and dam width, respectively. V_d and V_u are the dam volume and lake volume, respectively. e is the erodibility of the dam material. b_d is the breach duration and q_b is the peak outflow rate.